KCI Concrete Journal
Vol. 13 No. 1 pp. 19-25, January 2001

A 3-D Finite Element Model For R/C Structures Based On Orthotropic Hypoelastic Constitutive Law

Chang-Geun Cho* Moon-Ho Park**

* Researcher, Ph.D., Research Institute for Disaster Prevention, Kyungpook National Univ., Korea
** Professor, Ph.D., Dept. of Civil Engineering, Kyungpook National Univ., Korea

(Received June 23, 2000, Revised December 11, 2000)

Abstract

Based on the orthotropic hypoelasticity formulation, a constitutive material model of concrete taking account of triaxial stress state is presented. In this model, the ultimate strength surface of concrete in triaxial stress space is described by the Hsieh's four-parameter surface. On the other hand, the different ultimate strength surface of concrete in strain space is proposed in order to account for increasing ductility in high confinement pressure. Compressive ascending and descending behavior of concrete is considered. Concrete cracking behavior is considered as a smeared crack model, and after cracking, the tensile strain-softening behavior and the shear mechanism of cracked concrete are considered. The proposed constitutive model of concrete is compared with some results obtained from tests under the states of uniaxial, biaxial, and triaxial stresses. In triaxial compressive tests, the peak compressive stress from the predicted results agrees well with the experimental results, and ductility response under high confining pressure matches well the experimental results. The reinforcing bars embedded in concrete are considered as an isoparametric line element which could be easily incorporated into the isoparametric solid element of concrete, and the average stress – average strain relationship of the bar embedded in concrete is considered. From numerical examples for a reinforced concrete simple beam and a structural beam type member, the stress state of concrete in the vicinity of the critical region is investigated.

***keywords** : reinforced concrete, orthotropic hypoelasticity, finite element method, triaxial constitutive law of concrete*

1. Introduction

The compressive strength of concrete is highly dependent on various confinements, and the axial compressive strength of concrete increases with the increment of confining stress. Under very high confining stresses, extremely high compressive strengths have been recorded. It raises a question that the stress state of concrete in a region of concrete structural members can be different from the uniaxial stress state by existing of biaxial and triaxial compressive region near the beam-column joint. From previous studies on the compressive strength of concrete in prism with several height/width ratios[1] and reinforced concrete beam-column members[2], it was known that the flexural response of structural member was highly dependent on multiaxial compressive stress state of concrete. In this viewpoint, ideally analytical models to simulate a three dimensional response of a complete reinforced concrete structures with all structural components affecting the response will be valuable. The need for developing such analytical models to predict reinforced concrete structural behavior relates to their desired supplemental capabilities to predict the sequence of events and modes of failure observed in the test specimens.

The purpose of this study is to present a three-dimensional finite element model for reinforced concrete structures based on an orthotropic hypoelasticity formulation. In the present model, the ultimate strength surface of concrete in triaxial stress space is described by the Hsieh's four-parameter surface, on the other hand, the different ultimate strength surface of concrete in strain space is proposed in order to improve the influence on increasing ductility in high confinement pressure. Concrete cracking behavior is considered as a smeared crack model with post-

cracking behavior. The steel bars embedded in concrete are considered as an isoparametric line element and the average stress and average strain relationship of the bar embedded in concrete is considered. Extensive research over the past three decades has led to a few constitutive models for concrete, which are based on the principles of continuum mechanics. The elasticity-based model is among the most popular constitutive relationships used in conjunction with the finite element analysis of concrete structures. The linear elastic model was adopted initially for the concrete in relation with the finite element analysis of reinforced concrete by Ngo and Scordelis (1967).[3] However, it can not identify the nonlinear response and path dependent behavior of concrete at higher levels of compressive loading. Based on the Cauchy elastic model, adopted by Popovics (1973)[4] and Ahmad and Shah (1982)[5], the performance of linear elastic model can be improved significantly by assuming a nonlinear elastic behavior. By Kotsovos, et al. (1978)[6] and Ottosen (1979)[7], the hyperelastic models for concrete have been formulated by simply replacing the elastic moduli with secant moduli. This type of formulation is independent of the deformation path in the sense that stresses are uniquely determined from the current state of strain, or vice versa. An alternative approach, a hypoelastic model, to overcome the above deficiency is to describe the material behavior in terms of increments of stress and strain using tangent stiffness. Based on hypoelastic model, Elwi and Murray (1979)[8] developed a stress-strain relationship for concrete under axi-symmetric stress conditions, which incorporates the equivalent uniaxial strain concept of Darwin and Pecknold (1977)[9]. In the present model, above hypoelastic model under axisymmetric stress conditons is extended to triaxial stress conditions with a 6×6 compliance matrix.

2. Concrete Model in Compression

2.1 Orthotropic Hypoelasticity

In structures where the stress state at every point is defined by three principal stresses, concrete can be characterized during loading as a nonlinear orthotropic medium with the directions of orthotropy coincident with the principal stress directions. In this approach, as developed by Elwi and Murray (1979)[8] for axisymmetric stress conditions, the incremental stress-strain relations of concrete in multiaxial stress state for an orthotropically anisotropic material can be written as

$$\{d\sigma\} = [C]\{d\varepsilon\} \tag{1}$$

where $\{d\sigma\}$ and $\{d\varepsilon\}$ are the vector of stress and strain increments, respectively, and $[C]$ is the constitutive matrix. The following constraints must be fulfilled to ensure the symmetric condition of the compliance tensor:

$$\nu_{12}E_1 = \nu_{21}E_2,\ \nu_{13}E_1 = \nu_{31}E_3,\ \nu_{23}E_2 = \nu_{32}E_3 \tag{2}$$

By incorporating the above conditions, consequently, the incremental stress-strain relations of concrete in the local coordinate system of axes (1, 2, and 3) in the explicitly symmetric form in Eq. (1) are

$$\{d\sigma\} = \{d\sigma_1 \quad d\sigma_2 \quad d\sigma_3 \quad d\tau_{12} \quad d\tau_{23} \quad d\tau_{31}\}^T$$
$$\{d\varepsilon\} = \{d\varepsilon_1 \quad d\varepsilon_2 \quad d\varepsilon_3 \quad d\gamma_{12} \quad d\gamma_{23} \quad d\gamma_{31}\}^T$$
$$[C] = \frac{1}{\Omega}\begin{bmatrix} C_{11} & C_{12} & C_{13} & 0 & 0 & 0 \\ & C_{22} & C_{23} & 0 & 0 & 0 \\ & & C_{33} & 0 & 0 & 0 \\ & & & G_{12} & 0 & 0 \\ sym. & & & & G_{23} & 0 \\ & & & & & G_{31} \end{bmatrix} \tag{3}$$

where,

$$C_{11} = E_1(1-\mu_{32}^2),\quad C_{22} = E_2(1-\mu_{13}^2),$$
$$C_{33} = E_3(1-\mu_{12}^2)$$
$$C_{12} = \sqrt{E_1E_2}\,(\mu_{13}\mu_{32} + \mu_{12}),$$
$$C_{13} = \sqrt{E_1E_3}\,(\mu_{12}\mu_{32} + \mu_{13}), \tag{4}$$
$$C_{23} = \sqrt{E_2E_3}\,(\mu_{21}\mu_{31} + \mu_{23}),$$

and

$$\mu_{ij}^2 = \nu_{ij}\nu_{ji} \tag{5}$$
$$\Omega = 1 - \mu_{12}^2 - \mu_{23}^2 - \mu_{31}^2 - 2\mu_{12}\mu_{23}\mu_{31} \tag{6}$$

and the subscripts 1, 2, and 3 stand for the axes of orthotropy; ε and γ are normal and engineering shear strains, respectively; E_i is the tangential modulus of elasticity with respect to the orthotropic direction i (i=1, 2, 3) ; ν_{ij} is the Poisson's ratio in direction i due to uniaxial stress in direction j (i, j=1, 2, 3); and G_{ij} is the shear modulus of elasticity in plane i-j which is assumed to be invariant with respect to transformation to any non-orthotropic set of axes which results in:

$$G_{12} = [E_1 + E_2 - 2\mu_{12}\sqrt{E_1E_2} - (\sqrt{E_1}\mu_{23} + \sqrt{E_2}\mu_{31})^2]/4$$
$$G_{23} = [E_2 + E_3 - 2\mu_{23}\sqrt{E_2E_3} - (\sqrt{E_2}\mu_{31} + \sqrt{E_3}\mu_{12})^2]/4 \tag{7}$$
$$G_{31} = [E_3 + E_1 - 2\mu_{31}\sqrt{E_3E_1} - (\sqrt{E_3}\mu_{12} + \sqrt{E_1}\mu_{23})^2]/4$$

2.2 Equivalent Uniaxial Strains

For the incremental stress-strain relation in Eq. (1), it is necessary to describe the determination of the nine incremental moduli. To this end, the concept of equivalent uniaxial strain, as proposed by Darwin and Pecknold

axial strain, as proposed by Darwin and Pecknold (1977)[9], is adopted in the material model. By the transformation of Eq. (1), the equivalent uniaxial strains $d\varepsilon_{ui}$ can be expressed in terms of the actual incremental strains $d\varepsilon_i$ as

$$d\varepsilon_{ui} = B_{i1}d\varepsilon_1 + B_{i1}d\varepsilon_1 + B_{i1}d\varepsilon_1,\ B_{ij} = \frac{C_{ij}}{E_i} \tag{8}$$

2.3 Uniaxial Stress-strain Curve and Poisson's Ratio

For the uniaxial compressive stress-strain relationship of concrete, as shown in Fig. 1, Saenz (1964)'s curve[10] is adopted to describe compressive ascending region of concrete. In compressive descending region of concrete, stress is reduced linearly, and concrete is failure if any point reaches at ultimate stress, f_f. On the other hand, a significant volumetric ex-pansion of concrete subjected to higher strains has been observed during experiments. Based on results reported by Kupfer et al.(1973)[11] the following equations are used to describe the variation of Poisson's ratio.

$$\nu = \nu_o\left[1 + (4 - 5\varepsilon/\varepsilon_c)^2\right],\quad \varepsilon_c \le \varepsilon < 0.8\varepsilon_c \tag{9}$$

$$\nu = \nu_o\left(3\varepsilon/\varepsilon_c + 2\varepsilon_f/\varepsilon_c - 5\right)/\left(\varepsilon_f/\varepsilon_c - 1\right),\quad \varepsilon_f \le \varepsilon < \varepsilon_c \tag{10}$$

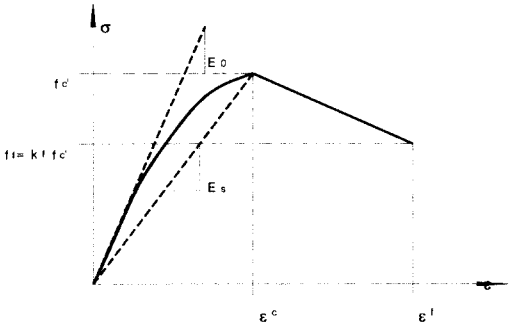

Fig. 1 Uniaxial stress-strain curve of concrete

2.4 Ultimate Strength Surface of Concrete

The ultimate strength surface of concrete in triaxial stress space is described in this study by the four parameter surface proposed by Hsieh et al.(1979)[12] and is expressed as,

$$f(I_1, J_2, \sigma_1) = a\overline{J_2} + b\sqrt{\overline{J_2}} + c\overline{\sigma_1} + d\overline{I_1} - 1 = 0 \tag{11}$$

where,

$$\overline{\sigma_1} = \frac{\sigma_1}{f_c},\quad \overline{I_1} = \frac{(\sigma_1 + \sigma_2 + \sigma_3)}{f_c} \tag{12}$$

$$\overline{J_2} = \frac{(\sigma_1 - \sigma_2)^2 + (\sigma_2 - \sigma_3)^2 + (\sigma_3 - \sigma_1)^2}{6(f_c)^2} \tag{13}$$

$$a = 2.018,\ b = 0.9714,\ c = 9.1421,\ d = 0.2312 \tag{14}$$

From the ultimate surface, the strength enhancement in triaxial state is modeled by modifying the peak stress of the uniaxial stress-strain curve as bellows

$$f_{ci} = \lambda_{si} f_c,\quad f_{fi} = \lambda_{si} f_f \tag{15}$$

where λ_{si} is so called the strength enhancement factor solved from the equation of ultimate surface. On the other hand, experiments have shown that concrete behaves more ductile for increasing confinement pressure. To account for increasing ductility in high confinement pressure, from experimental results by Kupfer, et al.(1969)[13] and Smith(1987)[14], the ductility enhancement is modeled as the function of the strength enhancement factor as

$$\lambda_{ei} = 0.3 + 0.7\lambda_{si}^2,\quad \lambda_{si} < 3$$
$$\lambda_{ei} = 5\lambda_{si} - 8.4,\quad \lambda_{si} \ge 3 \tag{16}$$

where λ_{ei} is so called the strain enhancement factor, and the enhanced strains at peak and ultimate stresses can be expressed as

$$\varepsilon_{ci} = \lambda_{ei}\varepsilon_c,\quad \varepsilon_{fi} = \lambda_{ei}\varepsilon_f \tag{17}$$

3. Concrete Model in Tension

Concrete cracking model is considered as a smeared crack approach. If the maximum principal stress for some reason exceeds a limiting value, a crack is assumed to form in a plane orthogonal to this stress. After this, the behavior of that zone of concrete becomes orthotropic. After cracking, new sets of cracks can be formed which are perpendicular to the previous cracks.

After concrete cracking, tensile stress is not immediately released to zero but is gradually released by strain-softening behavior. In this paper, as proposed by Yamaguchi, E. et al. (1990)[15], after concrete cracking, the stress-strain relation is considered as a linear strain-softening model. The total strain increment $\Delta\varepsilon$ is decomposed into two parts, the concrete strain increment $\Delta\varepsilon_{co}$ and the crack strain increment $\Delta\varepsilon_{cr}$, and the strain-softening modulus E_t can be derived as follows,

$$E_t^{-1} = E_o^{-1} + C_{cr}^{-1} \tag{18}$$

$$C_{cr} = -(f_t^2 w_f)/(2G_f) \tag{19}$$

where G_f is defined as the fracture energy of concrete required to create one unit of area of a continuous crack and w_f is the crack band width.

Experimental results indicate that a considerable amount of shear stress can be transferred across the rough surfaces of cracked concrete, due to the influences of the aggregate interlocking, reinforcement ratio and bar size. A common procedure to account for aggregate interlock in a smeared crack model is to attribute an appropriate value to the cracked shear modulus G_c as a function of the uncracked

shear modulus G. In the present work, from Kolmar, W. et al.(1984)[16], if strain exceeds tensile strain ε_t, the cracked shear modulus is assumed to be reduced as

$$G_c = \alpha_c G(1 - \varepsilon/\varepsilon_m), \quad \varepsilon_t \le \varepsilon < \varepsilon_m \tag{20}$$

where, α_c is used as 0.5 for one crack and 0.25 for over two cracks, and ε_m is used as 0.002.

4. Comparison with Test Results

Uniaxial, biaxial and triaxial stress-strain relationships obtained from the foregoing model are compared with the experimental results by Kupfer, H., et al.(1969) as shown in Figs. 2-3 and Smith, S. H.(1987) as shown in Figs. 4-6, respectively. These are also to be compared with predicted results by Han and Chen (1985)(17) and Selby (1993)(18). The uniaxial compressive strength of concrete is 32MPa for uniaxial and biaxial tests by Kupfer, H., et al.(1969), and 34.7MPa for triaxial tests by Smith, S. H.(1987).

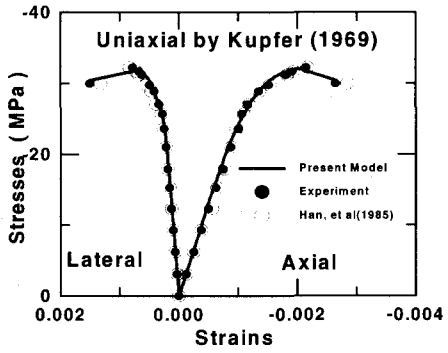

Fig. 2 Uniaxial compressive test

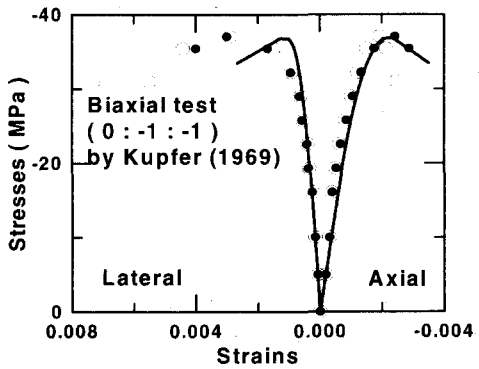

Fig. 3 Biaxial compressive test

As could be seen, the peak compressive stresses from predicted results by present model in all cases show a good agreement with that from the experimental tests.

To compare with other analysis result by Selby (1993), ductility response in compressive ascending portion is closer to the experimental results.

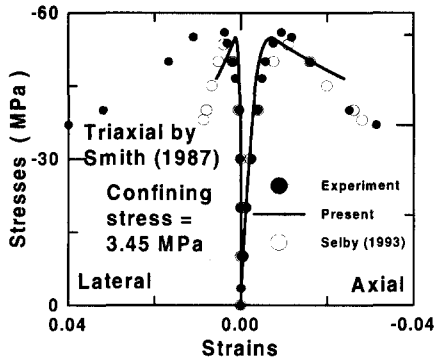

Fig. 4 Triaxial compressive test (3.45MPa)

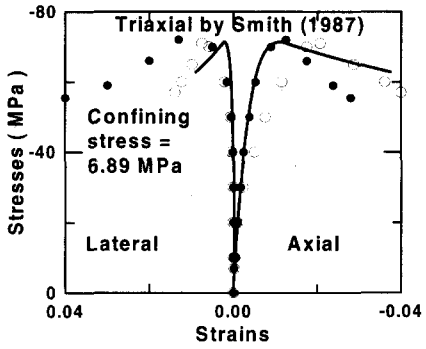

Fig. 5 Triaxial compressive test (6.89MPa)

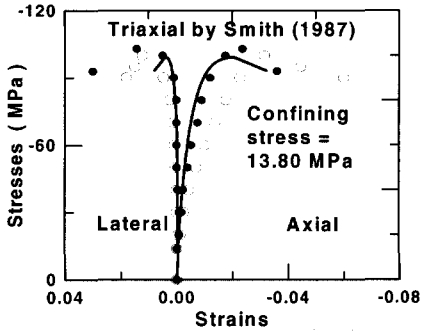

Fig. 6 Triaxial compressive test (13.8MPa)

However the response in compressive descending portion is somewhat different from the experimental results. It is mainly due that the strength and strain enhancement factors are used as same values respectively at both the peak stress point and the crushing point.

5. Modeling of Reinforcing Bars

The reinforcing bar is considered as a 2-noded isoparametric bar element to resist only axial force in the bar direction. Isoparametric bar element can be easily matched by placing them on solid elements. A bilinear idealization is adopted in order to model the elasto-plastic stress-strain relationships. It is assumed that between steel reinforcement and concrete is perfectly bond in the present study. On the other hand, in the case of tensile steel embedded in concrete, since the steel stress remains lower than the

yield strength everywhere else besides the vicinity of the crack plane, the average strain of the bar does not exhibit a yield shelf as does a bare bar. The strain-hardening rate is dependant on the average steel stress at the start of yielding, and is higher when the stress is lower. In present model, in order to model the post-yielding constitutive laws for a bar embedded in concrete, the average stress and average strain relationship proposed by Okamura and Maekawa (1991)[19] is adopted.

6. Numerical Examples

Based on the detailed descriptions in the previous sections, a three-dimensional finite element program for reinforced concrete structures, NFERC4P, was developed. The 8-noded hexahedral elements were used to model concrete solids. Nonlinear problem is solved by the modified Newton-Raphson approach. Tangential stiffness matrix is recalculated for each load increment or when the concrete newly cracks. Convergence criteria in terms of incremental nodal displacements are adopted in order to terminate the iterative cycle when the solution is considered to be sufficiently accurate.

6.1 Simple Beam Model

Using proposed program in the present study, an example model for reinforced concrete simple beam subjected to 3-point transverse load experimentally tested by Bresler and Scordelis (1963)[20] is analyzed. It was known that the experiment determined failure due to shear. The geometry and reinforcement details and its finite element mesh generation are illustrated in Fig. 7. Taking advantage of the symmetry, only half of the specimen was considered in the analysis. The beam has four tensile longitudinal bars without compressive and web reinforcements.

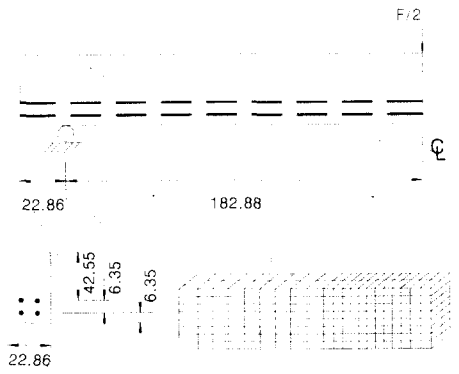

Fig. 7 Model of RC simple beam

Material properties of concrete were assumed to be as follows; uniaxial compressive strength f_c' of 22.5 MPa and its corresponding strain ε_c of 0.002, uniaxial tensile strength f_t of 2.25 MPa, ultimate strain ε_f of $4\varepsilon_c$, k_f of 0.75, initial Young's modulus E_0 of 20,000 MPa, initial Poisson's ratio ν_0 of 0.19, G_f of 250 N/m. Properties of reinforcing bars were as follows; yield stress f_y of 444.0 MPa, Young's modulus E_s of 200,000 MPa, modulus of strain-hardening E_{sh} of 2,000 MPa, diameter of 28.9 mm for a bar.

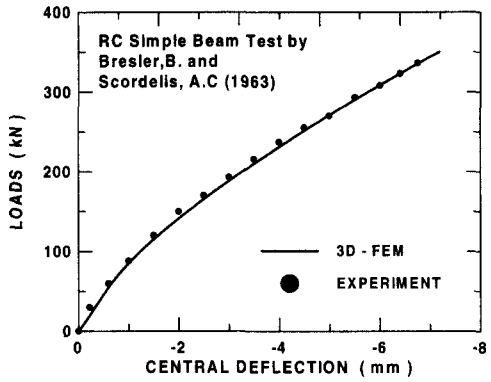

Fig. 8 Load-displacement at center

The load-displacement curve at mid-span for the Bresler-Scordelis beam predicted by the finite element method is compared to the experimental curve in Fig. 8. As can be seen from the figure the curves are essentially identical up to the experimental failure load. The analytical failure is recorded at a load level of 352 kN due to crushing of the concrete at the top. Experimentally observed ultimate load is 334 kN which is 5.8% lower than the ultimate load predicted by the finite element analysis.

Longitudinal tensile steel bar has not yield both in experimental and analytical results. The maximum tensile strain in present analysis is 0.00163 for lower reinforcement and 0.00126 for upper reinforcement.

Fig. 9 Analytical crack pattern

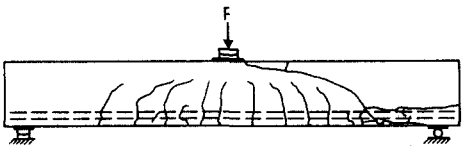

Fig. 10 Experimental crack pattern

The analytical crack pattern at early stages of cracking and near failure load respectively predicted in the present study is shown in Fig. 9, and the experimental crack pattern is shown in Fig. 10. Vertical cracks are seen at the center of the beam where flexure and shear are present. But towards the support the cracks are inclined due to the dominance of shear, and this same tendency is also observed from the experimental crack pattern. As can be seen both from analytical and experimental crack patterns, shear cracking is mainly contributed to the failure.

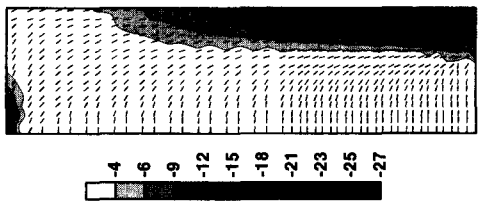

Fig. 11 Principal compressive stress (MPa)

Fig. 11 shows the contour of principal compressive stresses and their directions on outer surface of specimen. As can be seen from the stress contours the top half of the member is in compression with maximum stress occurring at the center of the beam, and the direction of principal compressive stress in the region is agreement with the member direction. Only except from the loading point, stresses in the overall region are below the uniaxial compressive strength of concrete.

6.2 Structural Beam Type Model

Another example for reinforced concrete structural beam member connected with beam-column joint at center is considered. The geometry and reinforcement detail and its finite element mesh generation are illustrated in Fig. 12. The cross-sectional dimension and material properties are same as the case of simple beam in previous section.

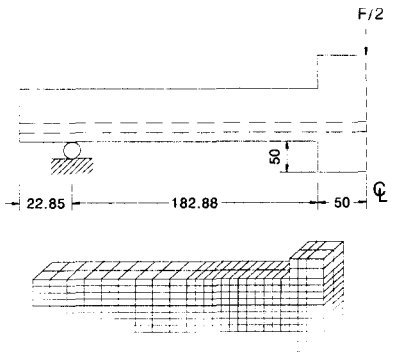

Fig. 12 Model of RC structrual beam

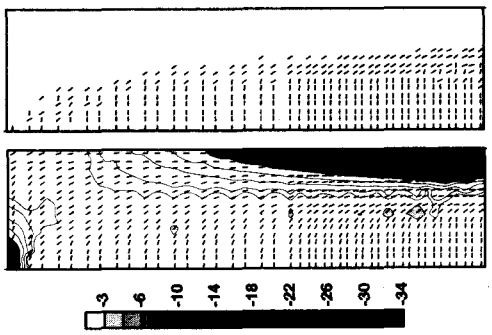

Fig. 13 Crack and Principal compressive stresses (MPa)

Fig. 13 shows the cracked pattern and the contour for principal compressive stress at failure load. The predicted crack pattern has the tendency that flexural cracking is dominant in the vicinity of the mid-span and diagonal cracking is also observed. It can be seen from the stress contour, concrete at top in the vicinity of beam-column joint is under severely high compressive stress state. The principal compressive stresses in the region highly exceed the uniaxial compressive strength of concrete.

Fig. 14 shows the distribution of cross-sectional stress both at joint and critical sections. The critical section is the first crushing point of concrete and is located at the cross-section of 72.6 mm away from the beam-column joint. At both sections, the peak compressive stresses of concrete exceed the uniaxial compressive strength of concrete. It shows concrete in the region behaves under a multiaxial compressive stress state. It is because that concrete in the region of connection is confined by the existence of beam-column joint. This influence, however, could not be seen in the case of simple beam.

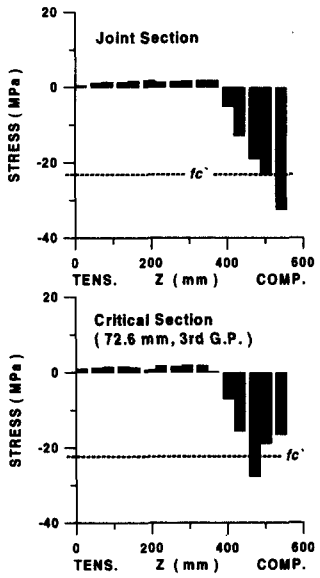

Fig. 14 Cross-sectional stress of concrete

7. Conclusion

Based on the orthotropic hypoelastic for-mulation for a triaxial constitutive relationship of concrete, a three-dimensional finite element model for reinforced concrete structures is presented. From proposed model and its analytical applications, the following conclusions are obtained.

In order to account for increasing ductility in high confinement pressure, a failure surface of concrete in strain space is proposed and the ductility response in high confining stress is well presented to compare with the experimental triaxial stress-strain relationship.

From numerical example for simple beam, concrete in the vicinity of critical region behaves dominant by the uni-

axial compressive stress state. However, in the case of structural beam type member, concrete in the critical region behaves dominant by the multiaxial compressive stress state. It is because that concrete in the region of connection is confined by the existence of beam-column joint.

References

1. Hotta, H., and Cho, C.G., "Three-Dimensional Finite Element Analysis On Compressive Strength of Concrete Prisms with Several Height/Width Ratios," J. Structural and Construction Engineering, Architectural Institute of Japan, No. 517, March 1999, pp. 115-123.
2. Hotta, H., and Cho, C.G., "Flexural Strength Analysis of RC Members Using Finite Element Models Taking Account of Triaxial Behavior of Concrete," J. Structural and Construction Engineering, Architectural Institute of Japan, No. 530, April 2000, pp. 115-121.
3. Ngo, D., and Scordelis, A.C., "Finite Element Analysis of Reinforced Concrete Beams," ACI Journal, Vol. 64, No. 3, March 1967, pp. 152-163.
4. Popovics, S., "A Numerical Approach to the Complete StressStrain Curve of Concrete," J. of Cement and Concrete Research, Vol. 3, No. 5, 1973, pp. 583-599.
5. Ahmad, S.H., and Shah, S.P., "Complete Triaxial StressStrain Curves for Concrete," ASCE, J. of Structural Division, Vol. 108, No. 4, 1982, pp. 728-742.
6. Kotsovos, M.D., and Newman, J.B., "Generalized StressStrain Relations for Concrete," ASCE, J. of Structural Engineering Division, Vol. 104, EM4, 1978, pp. 845-856.
7. Ottosen, N.S., "Constitutive Model for Short-Term Loading of Concrete, ASCE, J. of Engineering Mechanics, Vol. 105, No. EM1, 1979, pp. 127-141.
8. Elwi, A.A., and Murray, D.W., "A 3D Hypoelastic Concrete Constitutive Relationship," ASCE, J. of Engineering Mechanics, Vol. 105, EM4, August, 1979, pp. 623-641.
9. Darwin, D., and Pecknold, D.A., "Nonlinear Biaxial Law for Concrete," ASCE, J. of Engineering Mechanics, Vol. 103, EM2, April 1975, pp. 229-241.
10. Saenz, L.P., "Discussion of Equation for the Stress-Strain Curve of Concrete by Desayi and Krishman," J. of ACI, Vol. 61, September 1964, pp. 1229-1235.
11. Kupfer, H.B., and Gerstle, K.H., "Behavior of Concrete under Biaxial Stresses," ASCE, J. of Eng. Mech., Vol. 99, No. 4, 1973, pp. 852-866.
12. Hsieh, S.S., Ting, E.C., and Chen, W.F., "An Elastic-Fracture Model for Concrete," ASCE, Proc. 3d Eng. Mech. Div. Spec. Conf., Austin, Texas, 1979, pp. 437-440.
13. Kupfer, H.B., Hildorf, H.K., and Rusch, H., "Behavior of Concrete under Biaxial Stresses," J. of ACI, Vol. 66, No. 8, 1969, pp. 656-666.
14. Smith, S.H., SRS Report, No. 87-12, Dept. of Civ. Arch. and Env. Eng., Univ. of Colorado, Boulder, 1987.
15. Yamaguchi, E., and Chen, W.F., "Cracking Model For Finite Element Analysis Of Concrete Materials," ASCE, J. of Eng. Mech., Vol. 116, No. 6, June 1990, pp. 1242-1260.
16. Kolmar, W., and Mehlhorn, G., "Comparison of Shear Formulations for Cracked Reinforced Concrete Elements," Int. Conf. on Comp. Aided Analysis and Design of Conc. Struc., Part I, Pineridge Press, Swanses, U. K., 1984, pp. 133-147.
17. Han, D.J., and Chen, W.F., "A Nonuniform Hardening Plasticity Model for Concrete Materials," J. of Mechanics of Materials, 1985, pp. 283-302.
18. Selby, R.G., "Three-Dimensional Constitutive Relations for Reinforced Concrete," A Thesis for the Degree of Doctor of Philosophy, Dept. of Civil Eng., Univ. of Toronto, 1993.
19. Okamura, H., and Maekawa, K., "Nonlinear Analysis and Constitutive Models of Reinforced Concrete," Gihodo, 1991.
20. Bresler, B., and Scordelis, A.C., "Shear Strength of Reinforced Concrete Beams, J. of ACI, Vol. 60, No. 1, 1963, pp. 51-73.